

# Sieve Tubes in Action

Michael Knoblauch and Aart J. E. van Bel<sup>1</sup>

Institute for General Botany and Plant Physiology, Justus-Liebig-University, Senckenbergstrasse 17, 35390 Giessen, Germany

**A method was designed for in vivo observation of sieve element/companion complexes by using confocal laser scanning microscopy. A leaf attached to an intact fava bean plant was mounted upside down on the stage of a confocal microscope. Two shallow paradermal cortical cuts were made in the major vein. The basal cortical window allowed us to observe the phloem intact. The apical window at 3 cm from the site of observation was used to apply phloem-mobile fluorochromes, which identified living sieve elements at the observation site. In intact sieve tubes, the sieve plates did not present a barrier to mass flow, because the translocation of fluorochromes appeared to be unhindered. Two major occlusion mechanisms were distinguished. In response to intense laser light, the parietal proteins detached from the plasma membrane and formed a network of minute strands and clustered material that aggregated and pressed against the sieve plate. In response to mechanical damage, the evenly distributed P plastids exploded, giving rise to the formation of a massive plug against the sieve plate. In case of mechanical damage, the parietal proteins transformed into elastic threads (strands) that extended throughout the sieve element lumen. Our observations cover the phenomena encountered in previous microscopic and electron microscopic studies and provide a temporal disentanglement of the events giving rise to the confusing mass of structures observed thus far.**

## INTRODUCTION

Since the discovery of sieve elements (SEs) by Theodor Hartig (1837), countless attempts have been made to elucidate their structure and mode of action. It was understood that SEs are involved in long-distance transport of photoassimilates (Hartig, 1860), but the mechanism of translocation had not yet been determined. Diffusion and protoplasmic streaming were discarded as potential mechanisms as soon as the transport velocities proved to be typically 50 to 100 cm hr<sup>-1</sup> (Canny, 1975). Currently, the most widely favored mechanism for long-distance transport through SEs is the pressure flow hypothesis (Münch, 1930).

One of the stumbling blocks to full acceptance of pressure flow as the mechanism of phloem translocation is the typical components of the SEs. In particular, those directly behind the sieve plates may obstruct mass flow. These bodies, originally designated as Schleim (slime) by Hartig (1854), were later rebaptized as P proteins due to their proteinaceous character. Another hindrance may be presented by transcellular strands observed by light microscopy (Thaine, 1961). Initially, the strands were considered to be membranous structures (Thaine, 1962) but later respected as P protein filaments enclosing "endoplasmic tubules" (Thaine, 1969). Their rhythmic contraction produced peristaltic waves to facilitate long-distance transport (Thaine, 1969).

In electron microscopic images, a parietal filamentous network that fully or partly plugged the sieve pores was observed (Robidoux et al., 1973; Johnson et al., 1976). These filaments sometimes transformed into longitudinally oriented strands in response to injury alone (Evert et al., 1969). Because electron microscopy studies did not produce any evidence for in vivo *trans*-SE strands, the strands as proposed by Thaine were considered to be artifacts caused by the preparation of the tissue (Evert et al., 1969, 1973; Johnson et al., 1976).

The debate between the proponents of mass flow and those who claimed the existence of structural barriers to mass movement prompted massive research efforts (for an overview, see Evert, 1990). It was learned that the cytoplasm of mature SEs of dicotyledons has an endoplasmic reticulum (ER), P plastids, mitochondria, and with few exceptions (Esau and Gill, 1972; Walsh and Popovich, 1977), proteins in several forms (e.g., Cronshaw and Sabnis, 1990). The presumptive occlusion of the sieve pores by fine P protein threads conflicted with the mass flow hypothesis and gave rise to the conception of the electroosmotic theory (Fensom, 1957; Spanner, 1958, 1970).

The ongoing discussion on the mechanism of phloem transport essentially hinges on one question. What is the in vivo structure of SEs? With reference to the occlusion of the sieve pores, many investigators have pointed out that the main obstacle to elucidate the in vivo structure of SEs is their extreme sensitivity to any kind of manipulation (e.g.,

<sup>1</sup> To whom correspondence should be addressed. E-mail aart.v.bel@bot1.bio.uni-giessen.de; fax 49-641-99-35119.

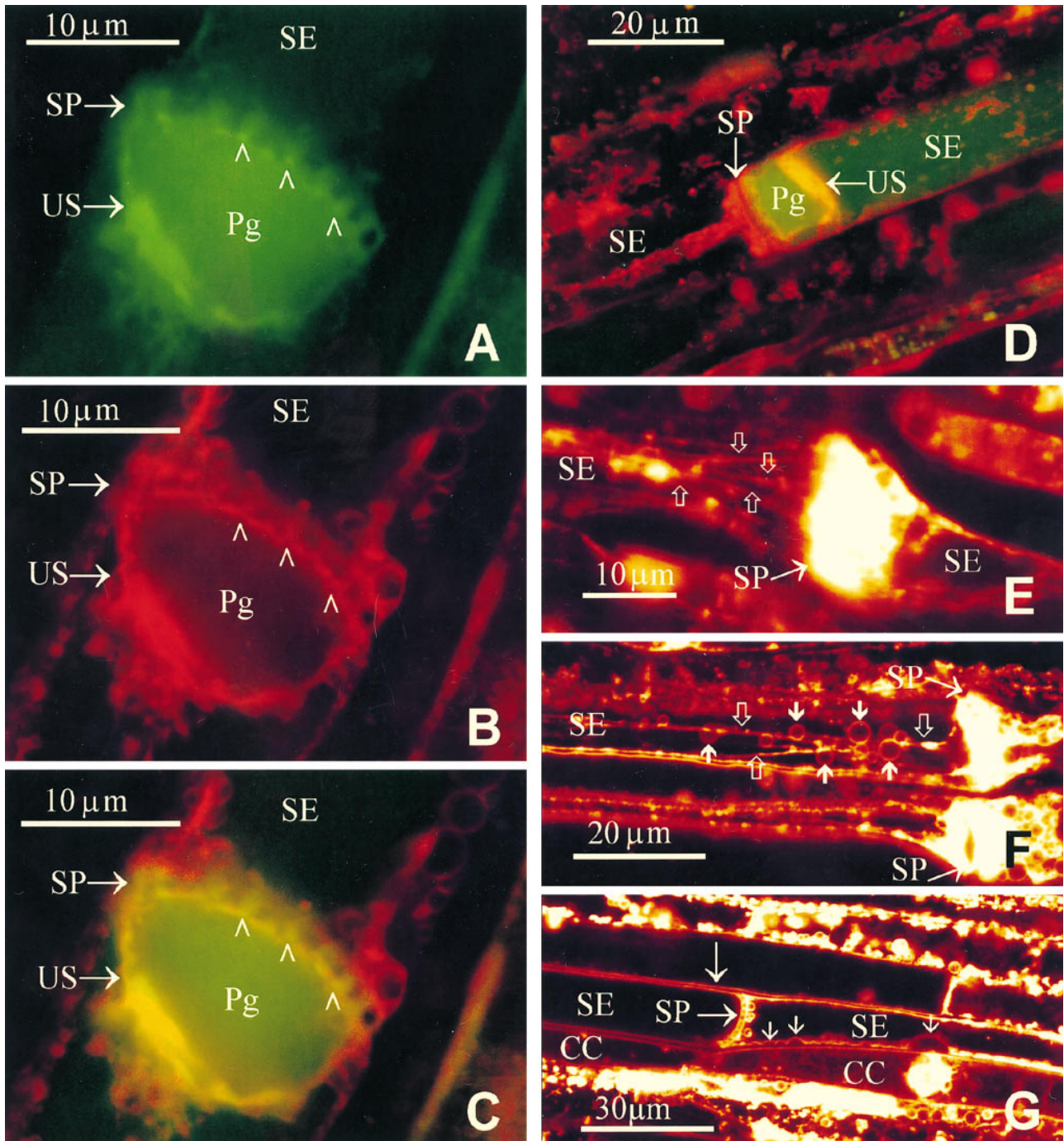


**Figure 1.** CLSM Images of SEs in Tissue Slices.

(A) to (C) Interpretation of the double staining of phloem tissue by differential fluorescence emission. (A) shows CDCFDA detection (excitation wavelength of 488 nm). A sedimentary plug in front of a sieve plate between two SEs was stained by CDCFDA. The plug has penetrated the sieve plate pores (arrowheads). An unknown intensely stained sediment is visible covering the plug. (B) shows RH-160 detection (excitation wavelength of 564 nm). The unknown sediment was more intensely stained by RH-160 than by CDCFDA. (C) is an overlay of the images in (A) and (B). Green-yellow indicates stronger staining by CDCFDA. Red-orange indicates stronger staining by RH-160.

(D) CDCFDA/RH-160 double stain detection. The left SE was cut and has lost its cytoplasmic content; only the cylindrical remnant of the plasma membrane is visible. The right SE has formed a massive plug in front of the sieve plate and a thick layer of unknown sediment. In the right SE, the plasma membrane stays in position.

wounding, cutting, or chemical fixation). The uncertainties with regard to SE ultrastructure have left their mark in the handbooks. The drawings are basically very indefinite, with the exception of the one in Kollmann (1973). This illustration presents a remarkably detailed portrait of the SE.

Our investigations have dealt with the visualization of the structure of undamaged and actually translocating SEs by using confocal laser scanning microscopy (CLSM). Use of various fluorescent dyes enabled us to observe intact SEs in whole plants mounted on the stage of the confocal laser scanning microscope. This study shows that intact SEs are essentially devoid of occlusions in the sieve pores and presents new insights into the origin, time scale, order of emergence, and triggering of the occlusion mechanisms.

## RESULTS

### Fluorochromes Brought into Action

A variety of fluorochromes was employed for confocal imaging of the structural components of the SEs in tissue slices and in actually transporting (i.e., living) sieve tubes in intact plants. For identification of intact SEs, membrane-permeant, phloem-mobile fluorescent probes were used. The general advantage of membrane-permeant fluorochromes is to avoid microinjection techniques that may inflict major cell damage (van der Schoot and van Bel, 1990).

Two of the phloem-mobile fluorochromes brought into action belong to the 5(6)carboxyfluorescein diacetate (CFDA) family. These dyes have in common that they cross the plasma membrane in acetate form and are cleaved by cytosolic enzymes producing membrane-impermeant carboxyfluoresceins (handbook from the manufacturer; Molecular Probes, Eugene, OR). CFDA has been used extensively in plant research as a marker for symplasmic transport (Grignon et al., 1989; Oparka et al., 1994). One of its derivatives, 5(6)-carboxy-2',7'-dichlorofluorescein diacetate (CDCFDA), has been used in yeast research (Roberts et al., 1991). To our

knowledge, CDCFDA has not been used in plant studies (CDCF was used by Yin et al. [1990]). In addition, we used 8-acetoxypyrene-1,3,6-trisulfonic acid trisodium salt (HPTSA), which has been described as a phloem-mobile symplasmic tracer having staining characteristics other than those of CFDA (Wright and Oparka, 1996).

The nonpolar RH dyes have been used for membrane staining in neurophysiological studies (e.g., Toth et al., 1993). The emission wavelength (705 nm) makes RH-160 an excellent candidate for double staining, with the phloem mobile tracers emitting green or yellow fluorescence. In this study, RH-160 was administered to stain the plasma membrane. Our attempt was successful. In addition, we discovered that RH-160 also tags itself to some nonmembranous components in plants, including the top layer of the SE-associated plugs in tissue slices (Figures 1B to 1D). In "injury" experiments, microelectrode tips were filled with sulforhodamin G or lucifer yellow CH (LYCH) to make the site of penetration visible under a confocal laser scanning microscope.

### CLSM of SEs in Tissue Slices; Identification of SE Components

In a first series of experiments, longitudinally cut slices of phloem tissue were treated with CDCFDA/RH-160 mixtures. The confocal laser scanning microscopic images of the slices were compared with those obtained with conventional light microscopy and transmission electron microscopy. The comparison aided in the identification of the cellular structures emerging in confocal images.

In keeping with the behavior of CFDA (Grignon et al., 1989; Wang and Fisher, 1994; Wang et al., 1994), CDCFDA passed through the plasma membrane of all cells but had the tendency to accumulate inside the sieve element/companion cell (SE/CC) complexes (Figure 1D). In contrast to CFDA—and the primary reason for its preference over CFDA—CDCFDA showed strong attachment to a sedimentary plug on the sieve plate that had penetrated the sieve plate pores (Figure 1A). The sedimentary plug seems to be composed of two layers (Figures 1A to 1D). The main body of the plug, moderately

**Figure 1.** (continued).

**(E)** RH-160 staining of a mechanically damaged SE (right) and an adjoining intact SE (left). In the right SE, a heterogeneous mixture of proteinaceous and membranous material is clogging the sieve plate. At left, SE strands (arrows) arising from the sieve plate fade away in the cytosolic lumen without any articulate parietal anchoring.

**(F)** An SE somewhat deeper inside the tissue, stained with RH-160. A lump of material is amassed at both sides of the sieve plate. Transparent vesicles (closed arrows) are attached to strands (open arrows) extending from the sieve plate through the lumen to the next sieve plate or to all margins.

**(G)** An SE in the interior of the tissue slice stained with RH-160. Strands or vesicles are absent. A few P plastids are visible lying against the sieve plate. The plasma membrane of the SE is locally detached from the cell wall (arrows).

CC, companion cell; Pg, plug; SE, sieve element; SP, sieve plate; US, unknown sediment.

stained by CDCFDA, may be of a proteinaceous nature (van Bel and Kempers, 1991; van Bel and van Rijen, 1994). The cover layer was strongly stained by CDCFDA and even more intensely by RH-160 (Figures 1A to 1D).

The nonpolar RH-160 turned out to be an excellent plasma membrane marker. The fluorochrome instantly associated with the plasma membrane of intact cells and to most membranous structures within the cells after 30 to 120 min (Figures 1E to 1G). Among them are the tonoplast and the membranous structures of chloroplasts, mitochondria (Figure 1G), and P plastids. Apart from the "established" membranous structures, vesicles of undetermined composition expanding in the SEs in response to injury (Figure 1F) were stained by RH-160.

As reported earlier (e.g., Hartig, 1854; Esau, 1969), the plugs always develop unilaterally onto the sieve plate (Figures 1A to 1D), probably due to a pressure release inside of the SEs. At the opposite sieve plate side, other structures develop commensurate with the degree of damage experienced (Figures 1D to 1G). SEs, which were actually cut, lost their cytoplasmic content (Figure 1D). What remains is an empty SE-plasma membrane cylinder that has become detached from the cell wall (Figure 1D). In the adjoining SE (the SE at right in Figure 1D), the cytoplasm stays in place (Figure 1E). In the latter SE and adjoining wounded SEs, strands had developed crossing the cytosolic SE lumen (Figure 1E). In severely wounded SEs, P plastids were never encountered.

In SEs, somewhat deeper inside a tissue slice, some strands extended through the cytosolic lumen from the one sieve plate to the other, whereas most strands branched away to the side walls (Figure 1F). The first species of strands may be the ones reported by Thaine (1961, 1969). Coincident with the appearance of the strands, vesicles emerged at both sides of the sieve plates. Most of the vesicles appeared on the side that was injured (Figure 1F). The formation of the vesicles building up from ~30 min after wounding seems to represent a slow response. In general, P plastids were absent in these SEs.

Visual observation of the middle part of the tissue by CLSM (up to 50 to 100  $\mu\text{m}$ , depending on the overlaying cell types) showed the absence of strands or vesicles in SE/CC complexes that were away from the transverse cuts. In these apparently less damaged SEs, a few P plastids pressed against the sieve plate were present, and the SE plasma membrane was locally detached from the cell wall (Figure 1G).

Nature and position of several SE components may be artifactual (i.e., subject to wounding responses). This probably holds true for most of the electron microscopic images published (artifact-inducing cutting precedes fixation). A tentative reconstruction of the wound reaction in successive SEs was made. This reconstruction was based on a broad range of observations in CDCFDA/RH-160-stained tissue slices. The diagram in Figure 2 (top) shows the structure of the SEs imposed by different degrees of injury. Triggering of the diverse structural reactions is discussed when the insights gained from the injury experiments are taken into consideration.

## How to Observe Intact SEs

As outlined in the Introduction, the *in vivo* structure is foremost for the assessment of the physiological potential of the sieve tubes. Because a paramount interest lies in the functioning of the phloem in intact plants, we designed a method to observe the SEs intact.

Cell sheets that were a few layers thick were sliced paradermally at two locations 3 cm apart from each other. Cell sheets were removed from the lower side of the main vein of mature broad bean leaves still attached to an intact plant (Figure 3). The two-site removal of overlaying tissues without disturbing the phloem allowed us to apply phloem-mobile fluorochromes in the vicinity of the SEs at the one site and to observe tracer translocation through living SEs by CLSM at the other (Figure 3). Use of the special high-magnification water immersion objective for CLSM had essential advantages. It enabled close visual access to the SEs without a glass cover that is necessary for oil immersion. The cover slip would also damage the surrounding tissues. In addition, the working distance of 220  $\mu\text{m}$  of the water immersion objective permitted the manipulation and impalement of microelectrodes under high-resolution surveillance.

At the site of application (Figure 3, position 2), the phloem-mobile tracers accumulated in all cell types but mainly in the SE/CC complexes. However, at the site of observation (Figure 3, position 1), fluorescence was only visible within the SE/CC complexes. The two-site approach made the SE/CC complexes stand out against the other cells and identified transporting (i.e., living) SEs. The direction of the dye movement was checked; CFDA only moved basipetally in the phloem (data not shown). In conclusion, CFDA was translocated in SEs, which are fully functional and most likely displaying the *in vivo* structure.

CFDA translocation usually needed 20 to 30 min to cover the distance of ~3 cm between the site of application and the site of observation. In this time interval, the fluorochrome must first have diffused through the apoplast of the overlying cells to the SE plasma membrane. After having crossed the plasma membrane of the SEs in the acetate form, CFDA was presumably hydrolyzed by esterases inside of the SEs (Goodall and Johnson, 1982). Following the chemical trapping inside of the SEs, the dye was dragged along with the pressure flow in the SEs (Grignon et al., 1989). The apparent rate of translocation in the SEs was affected by the massive accumulation of CFDA in the CCs along the translocation path (Figures 4C and 4D). This, in combination with the gradual entrance of CFDA into the SEs, made the absence of a distinct front of fluorescence quite logical. The slow emergence of fluorescence in SEs under observation met this expectation (Figure 4A). In view of the distance traveled by the dye and the intensity of the fluorescence (Figure 4B), the speed of movement must have been far more than 625  $\mu\text{m}$  (the frame of the image) per minute, which excludes diffusion and provides additional evidence for mass flow in the SEs being driven by a pressure gradient.

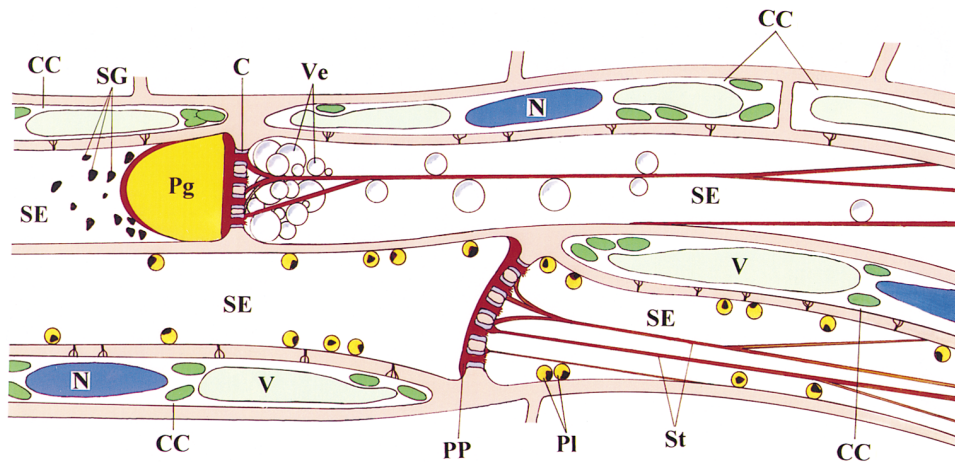


**Figure 2.** Structure of SEs Exposed to Different Degrees and Forms of Injury.

The direction of translocation before injury was from left to right. The nature of the structural responses depends on the degree of injury and the time frame of observation. The upper SE presents a strong response, mostly arising in the regions near the transverse cutting surface in tissue slices. A composite double-layered plug topped off by starch grains has been formed in front of the sieve plate. The location of the plug is dependent on the degree of injury. The plug is mostly formed at the sieve plate side facing the translocation stream. In case of extreme damage (at the very cutting edges), however, plugs are formed at the sieve plate side distal to the site of injury due to surging as a result of pressure loss. At the other side of the sieve plate, proteinaceous strands may or may not extend from one to the other end of the SE. The strands often branch to the side walls. In case of severe injury, the strands are absent; they have probably been torn away by the force of the pressure release and have sedimented on the plug. Vesicles building up from ~30 min after injury are attached to the strands, often in the vicinity of the sieve plate. P plastids as well as parietal proteins are absent. The lower sieve tube shows the response to high intensities of laser light. The parietal proteins produce a network of strands that deposit to variable degrees on the side of the sieve plate facing the mass flow stream. The P plastids remain intact and are located parietally. The emergence of vesicles has never been observed. C, callose; CC, companion cell; N, nucleus; Pg, plug; PI, P plastid; PP, parietal protein; SE, sieve element; SG, starch grain; St, strand; V, vacuole; Ve, vesicle.

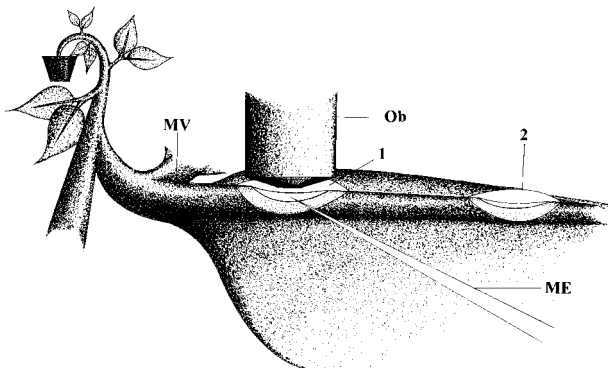


**Figure 3.** In Situ Observation of Functional SEs in Intact Plants.

Two cortical windows were paradermally sliced down to the phloem at the lower side of the main vein of a mature leaf attached to an intact plant. The apical window enabled the application of phloem-mobile fluorochromes. After translocation of the fluorochromes through the sieve tubes, the basal window allowed identification of fluorochrome-labeled intact SEs, previously stained with RH-160. The  $\times 63$  water immersion objective with a working distance of 220  $\mu\text{m}$  permitted the impalement of microelectrodes of various sizes while observing the target SEs. 1, basal cortical window; 2, apical cortical window; ME, microelectrode; MV, main vein; Ob, water immersion objective.

### In Vivo Structure of the SE/CC Complex

Optical sectioning at two levels through the same vascular bundle underlined that CFDA is moving exclusively in the sieve tubes (Figures 4C and 4D). Translocated CFDA obviously remained restricted to the SE/CC complexes (Figures 4A to 4D); no fluorescence unloading into the adjoining cell elements was detected. Apart from the starch grains in the P plastids, visible as minute bright spots in the SEs (Figures 4C and 4D), none of the cellular components of the SE/CC complexes was stained by CFDA. Detailed pictures of actually transporting SEs showed a homogeneous distribution of CFDA in the SEs and a stronger but unevenly distributed accumulation of fluorochrome inside of the CCs (Figures 4C and 4D). The dye preferentially accumulated in the lobed vacuole of the CCs, demarcating the location of the nuclei. The images illustrate the coincident ending of SEs and CCs and the staggered position of the CCs (Figures 4C and 4D), as was observed for SE/CC complexes of *Lupinus* and *Vicia* labeled with intracellularly injected LYCH (van Bel and van Rijen, 1994; van Bel, 1995). CFDA did not seem to accumulate in front of the conspicuous sieve plates, suggesting a free passage of solutes through the sieve pores (Figure 4C).

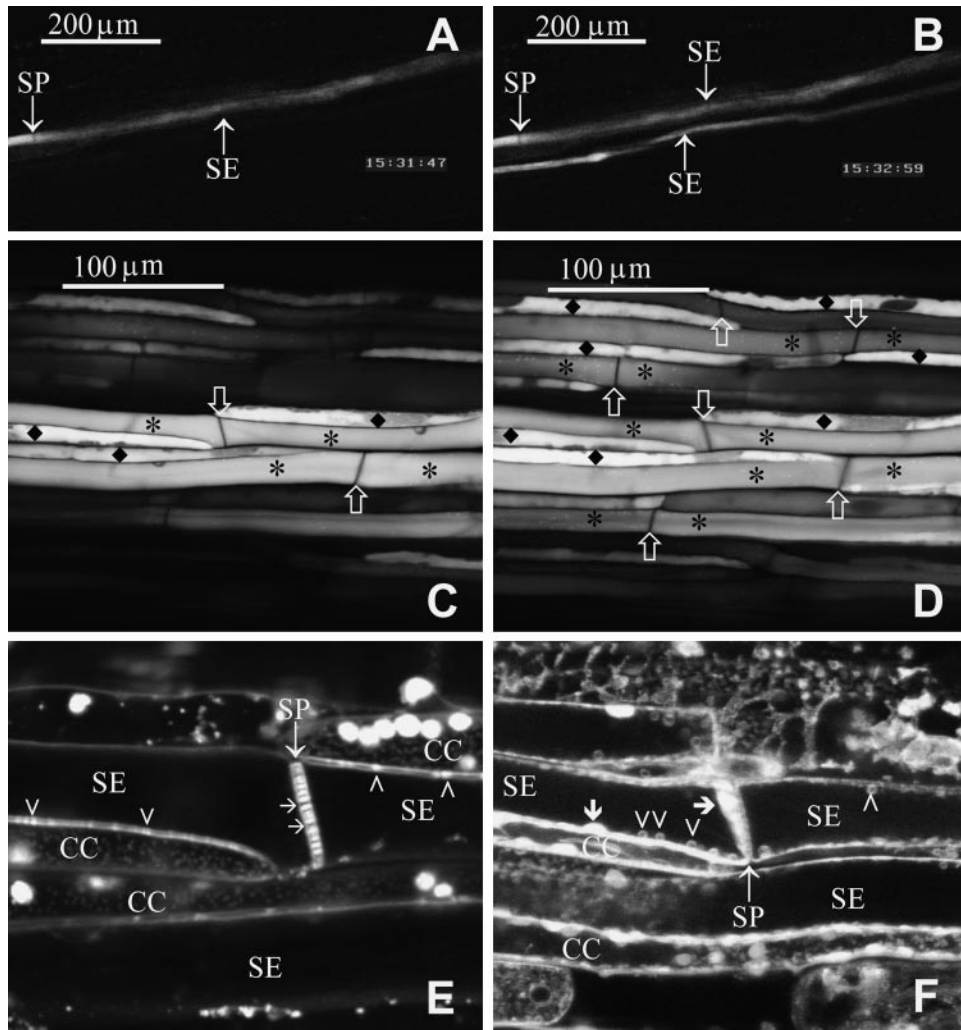


**Figure 4.** CLSM of Living Actually Translocating SEs.

The direction of fluorochrome translocation is from right to left in (A) to (F).

(A) and (B) Translocation of CFDA through intact phloem. In (A), the dye has already passed the image frame in one sieve tube. (B) shows the specimen in (A) 72 sec later. A second sieve tube has become highly fluorescent. The distance traveled by the dye and the intensity of the fluorescence are indicative of the rate of mass flow.

(C) and (D) High magnification of translocating SEs obtained by use of a  $\times 63$  water immersion objective. In (C), CFDA remains restricted to the SEs (asterisks) and the CCs (diamonds). Apparently, CFDA moving through the SEs strongly accumulates in the CCs. The sieve plates (arrows) demarcate the SEs. (D) is a deeper optical section through the same phloem bundle. The dye is evenly distributed over the SE. The dye accumulates in the vacuoles of the CCs, exposing darker central (nucleus) and parietal (cytoplasm) regions. Starch grains in the P plastids are visible as minute bright spots.

(E) Intact phloem tissue after 15-min staining with RH-160. No fluorescence-labeled substances have shown up inside of the SE. Sieve plate pores (arrows) are not occluded. Pore plasmodesma units (arrowheads) between the SEs and the adjoining CCs are stained clearly. Chloroplasts and probably mitochondria are visible in the CCs.

(F) Intact phloem tissue after 1-hr staining with RH-160. P plastids (arrowheads) are located along the plasma membrane of the SE and are evenly distributed. Parietal proteins line the plasma membrane of the SE with local thickenings (arrows). A thick layer of parietal protein is deposited onto the sieve plate.

CC, companion cell; SE, sieve element; SP, sieve plate.

After 15 min of staining the phloem with RH-160 at the site of observation, the membrane lining of the SEs was clearly visible (Figure 4E). The SEs appeared to be devoid of the subcellular structures (Figure 4E), as observed in injured tissues (Figures 1E and 1F); plugs, strands, and vesicles were absent. The plasma membrane of the SE could be observed crossing the sieve pores (Figure 4E). The pore plasmodesma units (Figure 4E) were more fluorescent at the CC side (the branched side with more plasma membrane material) than at the SE side (the single-pore side).

After prolonged treatment (1 hr) with RH-160, stained particles emerged inside the SEs, which implies that RH-160 is membrane permeant (Figure 4F). In the CCs, numerous small (probably mitochondria) and larger (probably chloroplasts) particles were visible (Figures 4E and 4F). In the SEs, parietal bodies (probably P plastids) showed up which are evenly distributed pressed against the plasma membrane (Figures 4F, 5B, and 6A).

Besides the P plastids, unequally distributed plaques of fluorescent sediment are parietally located (Figures 4F, 5A, 5B, and 6A). It appeared that RH-160 (Figures 4F and 5B) and CDCFDA (Figure 5A) labeled the same sediment. The sieve plate is largely free from sediment, apart from scattered aggregations, as shown by double-staining experiments in which the SEs were distantly labeled (by applying at position 2 in Figure 3) with HPTSA and locally labeled (position 1 in Figure 3) with RH-160 (Figure 5B). The massive CDCFDA-tagged plugs, which were observed on sieve plates in tissue slices (Figure 1D), were absent in the intact SEs (Figures 4E, 4F, 5A, and 5B). Occasionally, a thicker fluorescent sediment on the sieve plate appeared (Figures 4F

and 5B). This sedimentary layer did not seem to prevent the passage of the phloem-mobile HPTSA (Figure 5B). Use of HPTSA revealed the existence of large spindle-shaped clusters of material (probably nondispersed crystalline P protein bodies) inside of the living SEs (Figure 5B).

### Effects of Laser Light on SE Structure

Because the mass of sediment on the sieve plates in intact SEs seemingly correlated with the length of the observation period, the effect of laser light on the deposition of material was studied. A CLSM time scan of an intact SE stained with RH-160 showed dramatic structural responses to an increase of the laser intensity (Figures 6A to 6D). After raising the laser energy flow rate from  $\sim 45$  to  $100 \mu\text{W}$ , parietal packets of stained material detached from the cell wall within a few seconds and produced opaque structures in the cytosolic lumen (Figures 6A and 6B). The particles all moved in the same direction (Figure 6C), apparently being dragged along with the mass flow inside of the SE. Within 1 min, the particles had been moved to the sieve plate, where they aggregated (Figure 6D). In places, the particles were held together by strandlike material that made an elastic and sticky impression (Figure 6C).

To approximate the rate of irradiation that provokes detachment and clogging of the parietal proteins (Figures 6A to 6D), laser energy flow rates were measured in the focus plane of the objectives. With an image size of  $625 \times 625 \mu\text{m}$  and at a laser energy flow rate of  $600 \mu\text{W}$ , which is calculated to represent a laser energy fluence rate of  $\sim 1500 \text{ W}$

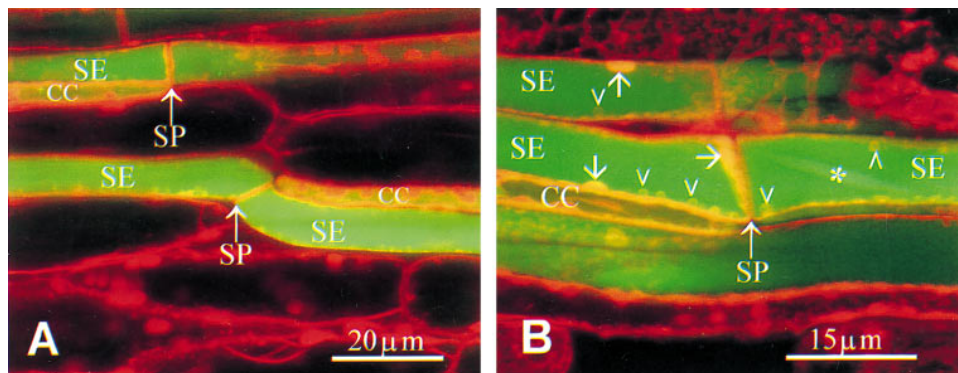


**Figure 5.** Double Stains of Living Actually Translocating SEs.

The direction of fluorochrome translocation is from right to left in (A) and (B).

(A) Double stain with locally applied RH-160 (red) and translocated CDCFDA (green). CDCFDA remains limited to the SEs and CCs. The sieve plates seem to be unplugged.

(B) Double stain with locally applied RH-160 (red) and translocated HPTSA (green). The parietal protein deposition (arrows) against the sieve plate does not impede the translocation of HPTSA. A crystalline P protein body (asterisk) is stained by HPTSA. P plastids (arrowheads) are parietally and evenly positioned.

CC, companion cell; SE, sieve element; SP, sieve plate.

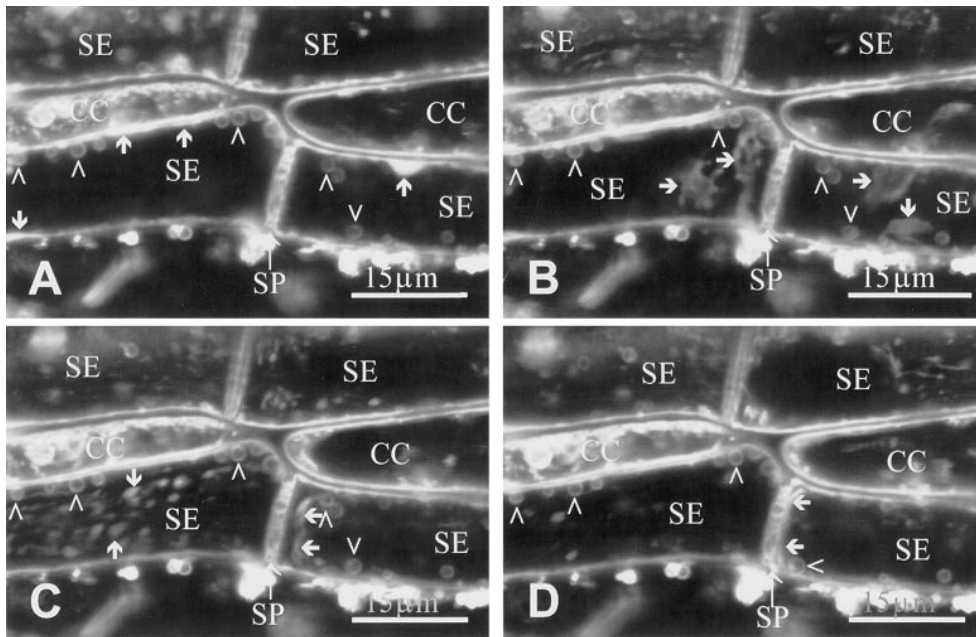


**Figure 6.** Response of Actually Translocating SEs to Intense Laser Light.

The direction of translocation is from right to left in (A) to (D).

(A) Time scan of an intact phloem region stained by RH-160. An SE with parietal proteins (arrows) and P plastids (arrowheads) viewed at laser light of low intensity.

(B) In response to a sudden rise in the laser light intensity, parietal proteins immediately detach from the plasma membrane and disperse into the cytosolic lumen of the SE (arrows). Note the formation of strands in the upper left SE and the intactness of P plastids (arrowheads).

(C) Mass flow drags the dispersed P proteins to the sieve plate. The proteins aggregate on the right side of the sieve plate. Opaque vesicular structures emerge in the left SE.

(D) One minute after the laser intensity is raised, a dense layer of detached material covers the sieve plate, and the vesicular structures in the left SE have moved in the direction of the next nonvisible sieve plate.

CC, companion cell; SE, sieve element; SP, sieve plate.

$m^{-2}$ , no effect on the translocation capacity of the SEs was observed for hours (Figures 4A and 4B). It should be noted that the calculations overestimate the energy fluence rates seen by the tissues, because medium and overlying tissues cause loss of intensity. A time scan of  $\sim 10$  min (Figure 4F), at an energy flow rate of  $45 \mu W$  representing  $7000 W m^{-2}$  at an image size of  $80 \times 80 \mu m$ , did not affect the ultrastructure of the SEs as well. Immediate effects were visible after raising the energy fluence rate to  $\sim 30,000 W m^{-2}$  (energy flow rate of  $100 \mu W$ , with an image size of  $61.2 \times 61.2 \mu m$ ; Figures 6A and 6B).

We wanted to determine whether the sedimentary layer occasionally observed in actually translocating SEs (Figures 4F and 5B) is an “in-borne” artifact of laser radiation. We believe that it is not for a number of reasons. (1) Under low laser intensity, proteinaceous sediment in intact SEs resided, if present at all, at either side of the sieve plate (Figures 4F and 5B). By contrast, sedimentation in SEs disturbed by intense laser irradiation always occurred at the side of the sieve plate facing the direction of the translocation stream

(Figure 6D). (2) Sediment, originally present at the other side of the sieve plate, was dislodged by intense laser irradiation and was swept away by the mass flow to the next sieve plate (Figures 6A and 6C). After detachment of the material, the sieve pores remained behind for awhile as empty spaces (Figure 6B). As a result, the detached material accumulated against the sieve plates in laser-irradiated SEs, whereas in unaffected SEs the sediment stays at all margins of the cell. (3) In phloem areas preexposed to intense laser light, translocation of phloem-mobile dyes was never observed, whereas fluorochrome movement was unhampered in the untreated adjacent regions (results not shown). This suggests a retardation of fluorochrome movement by the sieve plate-associated sediments in SEs impaired by intense radiation.

#### Effects of Mechanical Injury on the SE Structure

Remarkably, the P plastids stayed unaffected by intensified laser radiation (Figures 6A to 6D). The responses to injury by

laser light and to mechanical damage may differ, also because of the absence of P plastids in mechanically damaged tissues (Figures 1D and 1E). To identify the processes involved in the response to mechanical damage, originally intact SEs were exposed to rate-controlled mechanical damage. This study comprised observations on the effects of impalement with microelectrode tips of various diameters on SE structure (Figures 7 to 9).

In intact SEs, the P plastids were evenly distributed and located against the cell wall (Figures 7A and 8A). As soon as a microelectrode (diameter of  $\sim 1 \mu\text{m}$ ) was introduced into an intact SE, the pressure was instantly released in the impaled SE. The pressure release was indicated by bending of the sieve plate immediately after impalement (Figure 7B). Simultaneously, all P plastids in the damaged SE and most P plastids in the adjoining SE exploded, leaving their fluorescent coats on the wall (Figure 7B). Logically, the burst of the P plastids was ascribed to the abrupt loss of pressure inside of the SE. Combined detection of CDCFDA and RH-160 in

the same SE (Figures 7C and 7D) revealed that penetration of the needle provoked the formation of a CDCFDA-tagged plug on the sieve plate within 1 min (Figure 7C). In the course of up to 5 min, the fluorescence of the plug intensified (Figure 7D), and additional fluorescent material of a different nature traveled to the plug (Figure 7D), giving rise to a composed sedimentary plug similar to the one on the sieve plates in tissue slices (Figure 1D). The question is whether the plug gradually condensed or whether the staining gradually intensified during the period of observation.

The harsh penetration of the microelectrode impeded sealing of the plasma membrane so that the fluorescent cytosolic content leaked out of the SE (Figure 7D). Apparently, the plug produced in the adjacent SE partly occluded the sieve plate, because some fluorescent material stayed within this SE (Figure 7D).

That the pressure release, and not a “wound reaction,” provokes the burst of P plastids was demonstrated by careful insertion of a microelectrode with a minuscule electrode

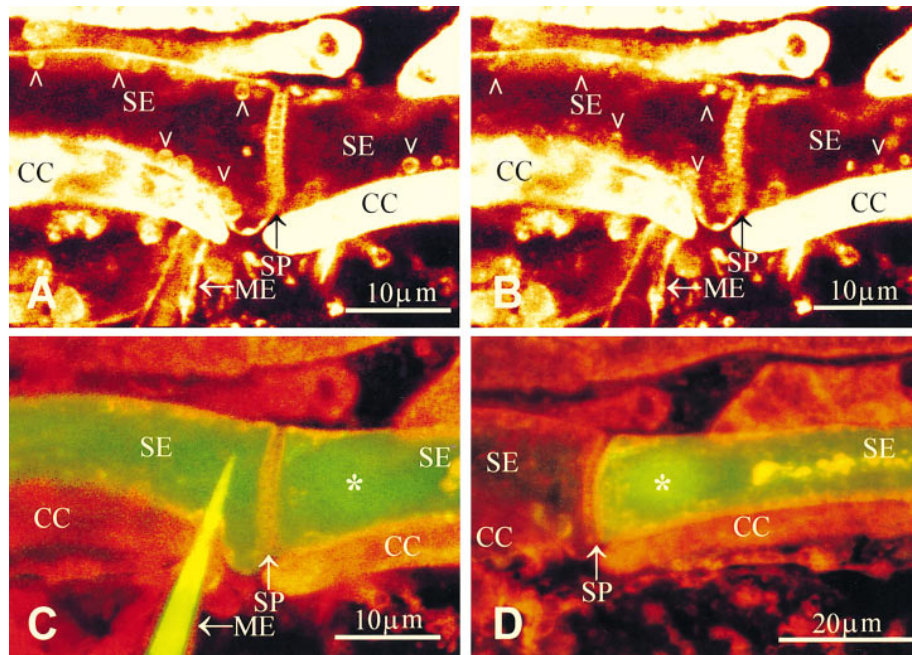


**Figure 7.** Reaction of Intact SEs to Injury Incurred by a “Medium Tip” Microelectrode.

The direction of fluorochrome translocation is from right to left in (A) to (D). A time scan of a phloem region stained by locally applied RH-160 and translocated CDCFDA is shown in (A) to (D).

(A) and (B) RH-160 detection. In (A), the translocating SEs with parietally positioned P plastids (arrowheads) are shown. The microelectrode is inserted into the CC of the left SE. In (B), after insertion of the microelectrode into the SE, all P plastids (arrowheads) immediately burst. The fragments of the P plastid membranes are visible as diffuse particles. After penetration of the microelectrode, the sieve plate curves toward the site of insertion, which is indicative of a sudden turgor loss in the wounded SE.

(C) and (D) RH-160/CDCFDA-LYCH double detection. The diameter of the microelectrode tip filled with LYCH is  $\sim 1 \mu\text{m}$ . One minute after insertion of the microelectrode, a massive plug (asterisk) becomes visible inside the right SE, as shown in (C). Three to four minutes after insertion of the microelectrode, the plug (asterisk) has become more intensely fluorescent, as shown in (D).

CC, companion cell; ME, microelectrode; SE, sieve element; SP, sieve plate.

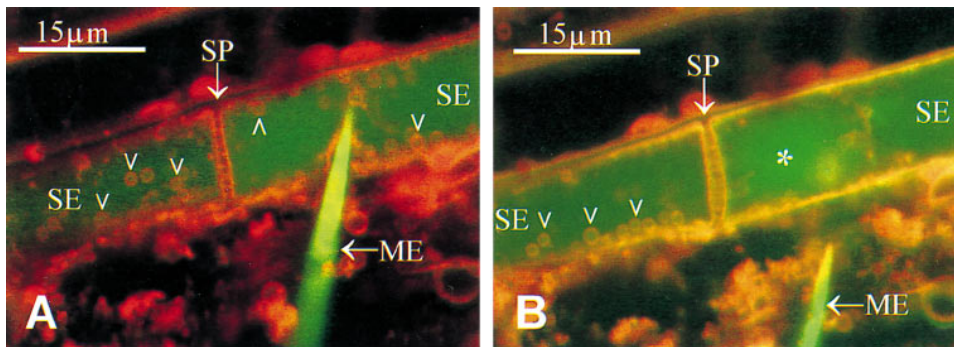


**Figure 8.** Reaction of Intact SEs to Injury Incurred by a "Small Tip" Microelectrode.

The direction of fluorochrome translocation is from right to left in (A) and (B). Time scans of an intact phloem region stained by locally applied RH-160 and translocated HPTSA, with double detection of RH-160 (red) and HPTSA (green), are shown. The tip diameter of the microelectrode filled with sulforhodamine G is  $\sim 0.1 \mu\text{m}$ .

(A) Careful insertion of the microelectrode into the right SE. The P plastids (arrowheads) remain intact, despite the penetration of the electrode. (B) After retraction of the microelectrode, the P plastids of the right SE explode, whereas the plastids of the left SE are still intact (arrowheads). In the right SE, a large plug (asterisk) builds up in front of the sieve plate. ME, microelectrode; SE, sieve element; SP, sieve plate.

tip (diameter of  $\sim 0.1 \mu\text{m}$ ). Insertion of such a microelectrode tip (Figure 8A) was not expected to cause any pressure release from the SE, provided that the plasma membrane sealing was perfect. Expectedly, the turgor pressure of the SE was insufficient to overcome the capillary forces inside of a tip of this size. Actually, P plastids remained intact during and after impalement into RH-160/HPTSA-stained intact SEs and no plug was formed (Figure 8A). As soon as the electrode was retracted, pressure appeared to be released through the small hole in the plasma membrane left behind by the electrode tip. The P plastids immediately exploded after withdrawal of the electrode, and the onset of a plug formation became visible (Figure 8B). The minor turgor loss had only local effects: the P plastids in the next SE remained intact (Figure 8B). The plugs provoked by mechanical damage did not bind to RH-160 (Figures 7D and 8B) in contrast to the sediment caused by laser irradiation (Figures 4F, 5B, and 6D).

After severe damage made by the penetration of a coarse microelectrode tip (diameter of  $\sim 10 \mu\text{m}$ ), a flexible and gradual response to injury was inferred from the behavior of four successive SEs (Figures 9A to 9C). The impaled SE (SE1) lost all CDCFDA, indicative of the loss of the cytosolic content. In the next SE (SE2), meanwhile, a plug had been built up that partly prevented fluorochrome leakage (Figure 9A). Before plugging the sieve plate, part of the SE content must have been lost. Fluorescence intensity of SE2 was appreciably lower than that of SE3; it was so much lower that the presence of CDCFDA in SE2 became invisible at a laser intensity sufficient to visualize CDCFDA in SE3 (Figures 9A and 9B). Moreover, sieve plate plugging was less massive, and some P plastids remained intact in SE3 (cf. Figures 9A

and 9B). Only a minor plug had been formed in SE4, whereas most P plastids were still intact (Figure 9C).

## DISCUSSION

### Identification and Localization of the Structural Components of Intact SEs

The phloem-mobile fluorochromes (CFDA, CDCFDA, and HPTSA) barely stained the structural components of intact SEs. The exceptions were CFDA labeling the starch grains in the P plastids (Figures 4C and 4D) and HPTSA labeling faintly large spindle-shaped bodies of proteinaceous material (Figure 5B). These bodies are likely identical to the massive P protein clusters, which are typical of Fabaceae. Electron microscopy of soybean (Fisher, 1975), runner bean (Lawton, 1978a), dwarf bean (Esau, 1978), and garden pea (Lawton, 1978b) revealed extensive protein aggregates.

Highly informative on the SE structure was the local application of RH-160, which originally was meant to visualize only the plasma membrane. The high resolution of the objective and the distinct fluorescence of the plasma membrane lining allowed us to observe the plasma membrane traversing the sieve plate pores and the pore plasmodesma units (Figure 4E).

Given the membranous nature of the P plastid coats, binding of RH-160 is logical on the assumption that RH-160 is slowly membrane permeant. As suspected by many investigators but never shown convincingly by using electron microscopy, P plastids are no doubt evenly distributed over

the plasma membrane in intact SEs (Figures 4F, 5B, 6A, 8A, and 10). A unique reconstruction from light microscopic images of sections of *Aristolochia* phloem (Kollmann, 1973) displayed a similarly even distribution of P plastids.

The assessment of the other parietal structures stained by RH-160 is difficult, because the initial assumption that RH-160 binds only to membranes does not seem to be true. The strands that emerge from the parietal proteins in mechanically damaged SEs (Figures 1E and 1F) are composed of nonmembranous material and yet stained by RH-160. The fluorescent material likely represents ER labyrinths or parietal proteins. Convoluted ER or appressed stacks of ER are abundant in the SEs of some species (Oparka and Johnson, 1978; Thorsch and Esau, 1981a), but impressive depositions of filamentous protein were located against the SE plasma membrane in other species (Evert et al., 1973; Giaquinta and Geiger, 1973; Fisher, 1975).

### Structure and Anchoring of P Plastids

P plastids are long-established organelles in the SEs of dicotyledons, the substructure of which is strongly species specific (Behnke, 1981). They are composed of a core or subcores of starchy and/or proteinaceous material in a matrix of aggregated proteins surrounded by a membrane (Behnke, 1981). It is probably the membrane of the P plastid that is stained by RH-160 (Figures 4F, 5B, and 6A). The P plastids in Fabaceae belong to the PIVcs- or S-type, which implies that the P plastid contains subcores of proteins and several starch grains (Behnke, 1981). In fava bean, one starch grain is much larger than the other ones (Figures 2 and 10; I. Dörr, personal communication). In spite of ubiquitous occurrence and detailed descriptions in numerous publications (e.g., see Behnke and Sjolund, 1990), the function of the P plastids remains obscure.

Our work seems to shed some light on the function of the P plastids. The injury experiments with microelectrodes of various diameters (Figures 6 to 9) demonstrate that a pressure drop in the SE cytosol triggers the disruption of the P plastids. In particular, the careful insertion and quick retraction of fine microelectrode tips (Figure 8) suggest that pressure release rather than the injury acts as the primary signal for wounding.

After explosion of the P plastids, the membranous fluorescent coats were still visible, attached to the wall, whereas the starch granules were recognizable near the sieve plate as particles faintly stained by CFDA (Figure 2). The liberated cores of starch were the particles often seen by light microscopy while making Brownian motion near the sieve plates of severed SEs (Esau, 1969; Barclay et al., 1977).

The consistent parietal location of the P plastids and their remnants indicates that the P plastids must be anchored in some way (Figure 4F). The attachment must be stable; time scans did not show any movement of the P plastids, and the basal plastid remnants did not displace after bursting (Figures

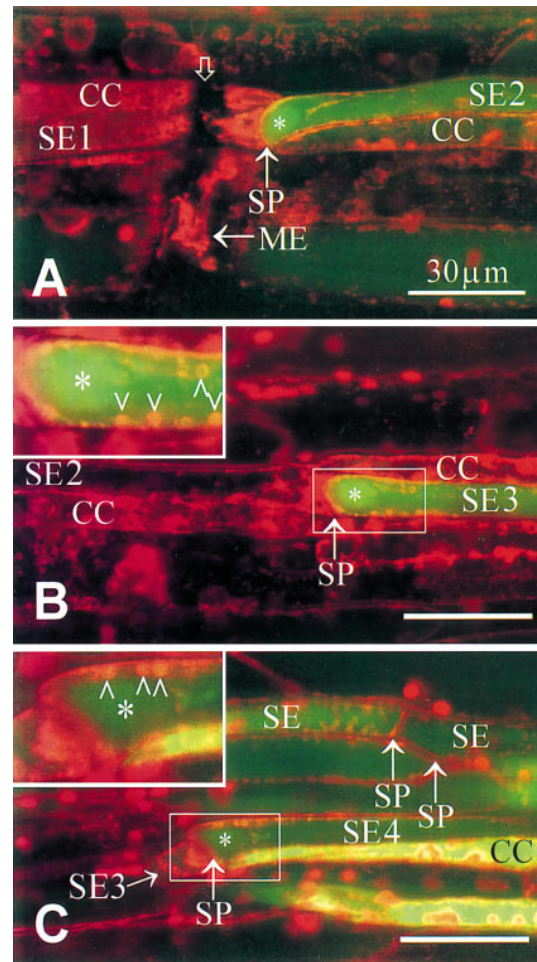


**Figure 9.** Reaction of Intact SEs to Injury Incurred by a “Coarse Tip” Microelectrode.

The direction of fluorochrome translocation is from right to left in (A) to (C). Double detection of locally applied RH-160 (red) and translocated CDCFDA (green) in four successive SEs (SE1, SE2, SE3, and SE4) after severe injury is shown. The tip diameter of the microelectrode is  $\sim 10 \mu\text{m}$ .

(A) The region around the sieve plate nearest to the site of injury (arrow). SE1 with its adjoining CC is completely disrupted by the piercing electrode. SE1 has lost all CDCFDA, which is indicative of the loss of the cytosolic content. SE2 has formed a massive plug (asterisk) that partly prevents the fluorescent solute to leak farther away. P plastids are absent in SE2.

(B) Region around the next sieve plate in acropetal direction under a much lower laser intensity than that shown in (A). SE3 shows a much stronger CDCFDA fluorescence than does SE2. A plug (asterisk) is present on the sieve plate. Some P plastids (boxed arrowheads) are still intact in SE3.

(C) Region around the third sieve plate in acropetal direction. A faintly stained plug (asterisk) covers the sieve plate. In SE4, more P plastids (arrowheads in box) are intact than in SE3. The fluorescence of CDCFDA in SE4 is not different from the adjacent uninjured sieve tubes. CC, companion cell; ME, microelectrode; SE, sieve element; SP, sieve plate.

6A to 6D and 7B to 7D). Electron microscopy actually showed P plastids attached to ER, which in turn may be continuous with the plasma membrane (Thorsch and Esau, 1981a, 1981b).

### Morphology and Definition of the Proteinaceous Compounds of the SEs

Location, form, and chemical nature of the proteins are very variable and obviously species specific. The complexity has been increased by the various degrees of damage response due to different preparation and fixation procedures. That several soluble proteins may turn into an insoluble form in response to injury further complicates the identification of the structures. The damage responses in our study can be assessed only when the structural proteins involved are defined properly.

At least 150 mainly low molecular weight proteins occur in the SEs (Fisher et al., 1992; Nakamura et al., 1993). Some are water soluble; others occur in a gelled state (e.g., Fisher et al., 1992). The nomenclature is confusing. P proteins are designated as being filamentous, fibrillar, tubular, crystalline, and amorphous, which might refer only to a specific state of aggregation (see various chapters in Behnke and Sjolund, 1990). In addition, a distinction is being made between parietal proteins and bodies of crystalline proteins. These P protein bodies may represent complex protein aggregates that have partly retained the stage of early development. There are

conflicting opinions as to whether crystalline proteins disperse into other morphological forms during SE differentiation (Wergin and Newcomb, 1970; Palevitz and Newcomb, 1971; Fisher, 1975; Lawton, 1978a). To make the terminology more confusing, filamentous P proteins were reported to occur in P plastids (Cronshaw and Sabnis, 1990). We could discriminate between proteinaceous materials only on the basis of their locations. Hence, we restrict ourselves to the terms parietal protein and P protein bodies, although we surmise that this distinction really neglects the complexity.

### Sieve Pores: Open or Plugged?

Spanner (1978) argued in his paper that sieve plate plugging made mass flow disputable as the mechanism of photosynthate translocation. As far as permitted by the resolution of CLSM, the sieve plates mostly appeared to be free of occluding substances (Figures 4E and 10). P plastids are parietally positioned, as is most of the proteinaceous material (Figures 4F, 5B, 6A, and 10). Occasionally, proteinaceous depositions were lying on the sieve plates (Figures 4F, 5B, and 10). However, the phloem-mobile fluorochromes did not accumulate in front of the sieve plates (Figures 4C, 4D, 5A, and 5B), suggesting that the sieve pores in intact SEs are essentially open (Figure 10). Because the molecular sizes of the fluorochromes are in the same order of magnitude as those of sugars, the present observations provide convincing support in favor of mass flow.

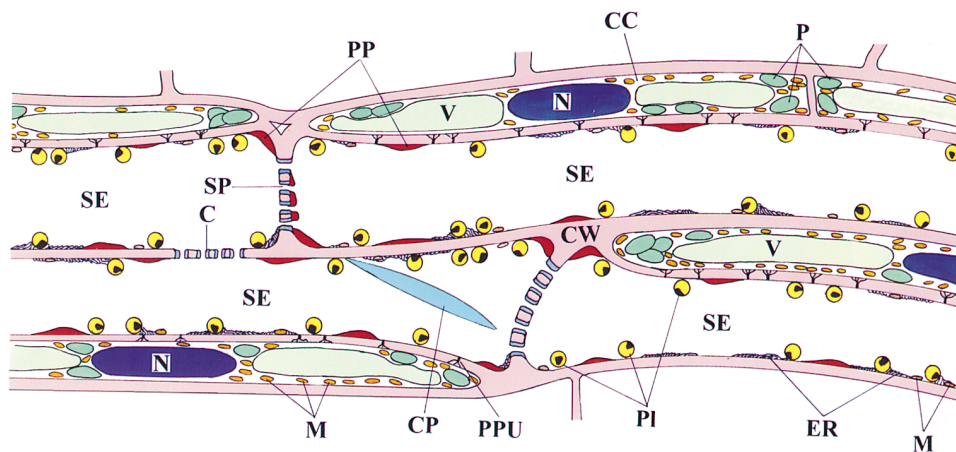


**Figure 10.** Reconstruction of the in Vivo SE Structure in Fava Bean.

Shown are sections of two sieve tubes with CCs, mostly in staggered position. SEs and CCs are mostly connected through numerous pore plasmodesma units. P plastids, mitochondria, and ER are parietally positioned and evenly distributed. Parietal proteins are locally aggregated. Parietal proteins and ER are sometimes located on the sieve plates or the margins of the sieve pores but do not impede mass flow. A large spindle-shaped crystalline protein cluster rests close to the sieve plate. The massive protein body is a specialty of the Fabaceae. C, callose; CC, companion cell; CP, crystalline protein body; CW, cell wall; ER, endoplasmic reticulum; M, mitochondria; N, nucleus; P and PI, plastids; PP, parietal protein; PPU, pore plasmodesma unit; SE, sieve element; SP, sieve plate; V, vacuole.

The restriction of the phloem-mobile probes to the SE/CC complexes confirms once again that the few plasmodesmata between the CCs and the phloem parenchyma (Kempers et al., 1998) present a symplasmic bottleneck. This symplasmic constriction was found in excised tissues (van der Schoot and van Bel, 1989; van Bel and Kempers, 1991; Oparka et al., 1992; van Bel and van Rijen, 1994; Kempers and van Bel, 1997) and in intact plants (Oparka et al., 1994; Rhodes et al., 1996). Under specific conditions, however, the plasmodesmata open up to most likely modulate the carbon flux in the plants (Hayes et al., 1987; Patrick and Offler, 1996).

### Response to Laser Light

Strong laser irradiation provokes detachment of the RH-160 reactive parietal sediment. RH-160 is reported to be a membrane marker and therefore would indicate detachment of stacked ER, which is abundantly present in the SEs of fava bean (I. Dörr, personal communication). Yet, we believe that the major part of the detached particles are parietal proteins for several reasons. (1) Thick and irregular packs of similar material were shown to be proteinaceous in several species (e.g., Evert et al., 1973), including fava bean (I. Dörr, unpublished results). (2) The material transforms into elastic strands that have been identified as proteins and not as membranous material in electron microscopy (Esau and Cronshaw, 1967; Johnson et al., 1976). (3) The extensibility and transformability of the fine threads which often connect the material during detachment from the original site of deposition (Figures 6A and 6C) give the impression that the material is elastic. That ER membranes are elastic to this extent is unlikely. (4) The P plastids, which may be connected to the ER (Thorsch and Esau, 1981a, 1981b), were not dislocated during the displacement of the fluorescent material. And (5) the mass of parietal proteins on sieve plates was inversely correlated with the amount of still parietally located proteins in other species (Esau, 1969; Evert et al., 1973; Giaquinta and Geiger, 1973; Robidoux et al., 1973; Fisher, 1975; Johnson et al., 1976).

The response to laser light intensities (Figure 6) likely does not reflect the behavioral reaction to natural light conditions. The intensities exceed by far the solar constant of  $1400 \text{ W m}^{-2}$ . The reaction of the SEs may be due to a rise in temperature imposed by the incident laser light and may express a defense mechanism against high temperatures. Incidentally, the results warn against unlimited laser radiation for the study of living cells.

### Response to Mechanical Damage

The reactions to mechanical injury and to laser light are clearly different. However, both may occur simultaneously, in particular when the damage is severe (Figure 2). The main

difference between the reactions lies in the bursting of the P plastids. The disruption of the P plastids is due to the pressure release in the SEs and not to immediate wounding responses (Figures 8A and 8B). That the P plastids set free coagulating substances is the most plausible explanation for the massive plug formation on the sieve plates, given the time frame and the order of events (Figures 7 to 9). In an earlier study in which P plastids were burst by iodine treatment, the liberated starch grains were hypothesized to play a role in sieve plate plugging (Barclay et al., 1977).

Most likely, the crystalline P protein body represents the nucleus of the plug formation in fava bean. The putative scenario of plug formation implies that dispersion of the P protein bodies should go along with breakage of the P plastids. Such a coincidence was confirmed by electron microscopic images of soybean (Wergin and Newcomb, 1970) and *Desmodium canadense* (Palevitz and Newcomb, 1971). In SEs of runner bean roots in which the P plastids were still intact, the material of the P protein bodies was not dispersed (Lawton, 1978a).

Apart from the coagulates from P protein material and P plastid content, the plugs also are composed of material from the parietal protein. This material was visible as a more intensely labeled layer on the primary plug (Figures 1A to 1D) and was connected by robust strands with the parietal plasma membrane regions. The strands that emerged in severely damaged SEs (Figures 1E and 1F) were also seen as bundles of P protein filaments in electron micrographs (Esau and Cronshaw, 1967; Johnson et al., 1976).

### Efficiency of the Plugging Reactions

In conclusion, P plastids explode in immediate response to pressure release in the SEs and set substances free that react with the P protein body material. The product is a conglomerate of substances that plug the sieve pores. Activated by the surge produced by the pressure release, parietal proteins are torn away or detach from the SE plasma membrane, building a cover layer on the developing plug (Figure 2). The elasticity and stickiness of the parietal material give rise to an irregular system of strands. The vigor of the pressure disturbance determines the morphology of the strand system (Figure 2).

The presence of parietal P plastids and ER (Figure 10) did not prevent mass flow in intact SEs (Figures 4F, 5A, and 5B). Hence, the deposition of parietal proteins on the sieve plates (Figures 6A to 6D) expectedly only retards solute passage through the sieve plate pores to some degree. When fluorescent dyes were injected into the SEs, depositions occurred, probably in response to the impalement of the microelectrode (van der Schoot and van Bel, 1989; van Bel and Kempers, 1991; Oparka et al., 1992; van Bel and van Rijen, 1994; Kempers and van Bel, 1997). Nevertheless, these massive plugs were easily permeable to fluorescent probes up to 4.5 kD (Kempers and van Bel, 1997). This

raises the question whether the plugging observed here fully seals the sieve plates. An alternative explanation might be that longitudinal movement of the probes is only possible during the time lapse between the onset of plug formation and the definitive occlusion of the sieve plate. In case of severe injury, the sieve plate appears to be tightly sealed for solutes after some time (Figures 9A and 9B). This sealing is probably complemented by extracellular deposition of callose in the sieve plate region (Evert and Derr, 1964).

## METHODS

### Plant Material

Pot plants of *Vicia fava* cv Witkiem major (Nunhems Zaden BV, Haelen, The Netherlands) were grown in a greenhouse under standard conditions of 20°C at 60 to 70% relative humidity during a 14-hr-day and 10-hr-dark period, with daylight plus additional lamp light (model SONT Agro 400 W; Philips, Eindhoven, The Netherlands) to a minimum irradiance of 250  $\mu\text{mol m}^{-2} \text{sec}^{-1}$  at plant level. Plants were used for experiments 17 to 21 days after germination.

### Preparation for Observation by Confocal Laser Scanning Microscopy

A few cortical cell layers were locally removed down to the phloem from the lower side of the main vein of a mature leaf. The layers were removed by manual paradermal slicing with a new Wilkinson razor blade (Figure 3, position 1), while avoiding damage of the phloem. Immediately after cutting a shallow window ( $\sim 10$  mm long and 2 mm wide), we bathed the free-lying phloem tissue in a medium with 10  $\text{mol m}^{-3}$  KCl, 10  $\text{mol m}^{-3}$   $\text{CaCl}_2$ , and 5  $\text{mol m}^{-3}$  NaCl in double-distilled water. To allow the cells to create their own apoplasmic environment, the medium was not buffered. The leaf was fixed in an upside-down position with two-side adhesive tape on a convex plastic slide. The state of the tissue was checked microscopically. If the phloem appeared to be undamaged, a second window (10  $\times$  2 mm), 2 to 3 cm acropetal from the first one, was manufactured (Figure 3, position 2) and bathed in the unbuffered medium mentioned previously. The convex slide carrying the leaf, still attached to the whole plant, was mounted on the stage of a confocal laser scanning microscope. The tissue windows were blotted just before application of fluorochrome solutions.

### Fluorescent Probes

To be used as phloem mobile tracers, 10 mg of 5(6)-carboxyfluorescein diacetate (CFDA; C-195) and 5(6)-carboxy-2',7'-dichloro-fluorescein diacetate (CDCFDA; C-369) were each dissolved in a minimum volume of 500  $\text{mol m}^{-3}$  KOH. The stock was diluted in double-distilled water up to 20 mL. KCl,  $\text{CaCl}_2$ , and NaCl were added to final concentrations of 10, 10, and 5  $\text{mol m}^{-3}$ , respectively. The pH was adjusted to 6.3 with 1000  $\text{mol m}^{-3}$  HCl.

As a phloem-mobile compound alternative to the CFDA derivatives, 8-acetoxypyrene-1,3,6-trisulfonic acid trisodium salt (HPTSA; A-396) was used, which was dissolved in double-distilled water to a

final concentration of 20  $\text{mg mL}^{-1}$ . KCl,  $\text{CaCl}_2$ , and NaCl were added to final concentrations of 10, 10, and 5  $\text{mol m}^{-3}$ , respectively.

Lucifer yellow CH, potassium salt (LYCH; L-1177) was dissolved in double-distilled water to a concentration of 7% (w/v). The dye was kept in darkness at 4°C for  $\sim 2$  weeks, during which the unsolubilized crystals sedimented. The supernatant was used for filling microelectrode tips. Sulforhodamin G (Aldrich, Milwaukee, WI) was dissolved in 0.1  $\text{mol m}^{-3}$  NaOH-Mes buffer, pH 6, to a final concentration of 0.01% and used for filling microelectrode tips.

For its use as a membrane stain, 25 mg of *N*-(4-sulfobutyl)-4-(4-(4-dibutylamino)phenyl)butadienyl)pyridinium inner salt (RH-160, S-1107) was solubilized in 1 mL of ethanol. Two microliters of the stock was added directly to the bathing medium. Apart from sulforhodamin G, all fluorochromes were purchased from Molecular Probes (Eugene, OR; the codes are from the 1996 catalog).

### Microscopy

Phloem tissue was examined with a Leica (Heidelberg, Germany) TCS 4D confocal laser scanning microscope. CFDA, CDCFDA, LYCH, and sulforhodamin G were excited by the 488-nm line produced by a 75-mW argon/krypton laser (Omnichrome, Chino, CA). The emission was observed by using a fluorescein band pass filter.

HPTSA was excited by the 488- and 476-nm lines of the argon/krypton laser. The emitted light was split by a 580-nm beam splitter, and short wavelengths were observed by using a 510-nm long-pass filter. RH-160 was excited by the 564-nm line of the 75-mW argon/krypton laser, and a 590-nm long pass filter was used for observation.

For two-channel scans with CFDA, CDCFDA, HPTSA, LYCH, or sulforhodamin G, on the one hand, and RH-160, on the other, the 488- and the 564-nm lines of the laser were used simultaneously for excitation. A 580-nm beam splitter passed the light to the two detector heads, and the appropriate emission filters were selected for observation. The observations were conducted with a PL Fluotar  $\times 16/0.50$  IMM objective (Leica; Figures 4A and 4B) or a PL APO  $\times 63/1.20$  W CORR objective (Leica; Figures 1, 4C to 4F, 5 to 7, and 9).

### Observation of the Tissues

In initial experiments, petiole slices were prepared in which phloem tissue was damaged to examine the effects of severe injury. The damaged tissue was stained with CDCFDA or RH-160. In subsequent experiments with intact plants, the apical window served the application of phloem-mobile fluorochromes, the basal one the administration of RH-160 and the observation of the phloem tissue. The movement of phloem-mobile fluorochromes was observed from  $\sim 30$  min after fluorochrome application at the apical window. The working distance of 220  $\mu\text{m}$  between objective and object left a space just large enough to insert microelectrode tips. The microelectrodes were advanced by a four-axis joystick micromanipulator (model MMW-204; Narishige, Tokyo, Japan) that was installed on the stage of the confocal laser scanning microscope in the upright configuration. The upright position enabled observation of intact plants and the fixed micromanipulator continuous focusing during the manipulation. The minute working distance required electrodes with a long strong shank and rapidly tapering tip. Microelectrodes with a fine (diameter of  $\sim 0.1$   $\mu\text{m}$ ) and medium (diameter of  $\sim 1$   $\mu\text{m}$ ) tip size were pulled from borosilicate glass capillaries (1 mm outer diameter, 0.58 mm

inner diameter with an inner filament; Clark Electromedical Instruments, Reading, UK) with a laser puller (model P-2000; Sutter Instruments, Novato, CA). The microelectrodes with a coarse tip (diameter of  $\sim 10 \mu\text{m}$ ) were manufactured by breaking the tip from 1- $\mu\text{m}$  microelectrodes.

### Measurement of Laser Energy Flow Rates

Laser energy flow rates and energy fluence rates (see Salisbury [1996] for definitions) in the focus plane of the objectives were measured by an LM-2 probe connected to a Fieldmaster photometer (Coherent, Palo Alto, CA) for different wave lengths at various laser intensities. Because of the quenching in the optical system of the confocal laser scanning microscope, the laser energy flow rate was calibrated for each objective separately.

### ACKNOWLEDGMENTS

All original images and a few extra time scans (movies) related to this article can be retrieved from the following internet page: <http://www.uni-giessen.de/gf1114/rgvbel/index.htm>. We extend our thanks to Denton Prior and Dr. Karl Oparka (Scottish Crop Research Institute, Invergowrie, Dundee, Scotland) for all forms of support during the confocal laser scanning microscope installation, Dr. Hubert Felle (University of Giessen) for assistance in fabrication of the microelectrodes, Guido Steude (University of Giessen) for measuring laser energy flow rates, Dr. Inge Dörr (University of Kiel, Germany) for providing us with unpublished work, Volkmar Thier and Sven Tränkner (Senckenbergische Naturforschende Gesellschaft, Frankfurt, Germany) for computer processing of the confocal laser scanning microscope images, Dr. H.-Dietmar Behnke (University of Heidelberg, Germany) and Dr. Alexander Schulz (University of Kiel) for helpful criticism, and Manfred Jung, Peter Schneider, and Dorothee Schroth (Leica, Bensheim, Germany) for continuous advice and support.

Received July 3, 1997; accepted November 19, 1997.

### REFERENCES

- Barclay, G.F., Oparka, K.J., and Johnson, R.P.C. (1977). Induced disruption of sieve element plastids in *Heracleum mantagazzianum* L. J. Exp. Bot. **28**, 709–717.
- Behnke, H.D. (1981). Sieve-element characters. Nord. J. Bot. **1**, 381–400.
- Behnke, H.D., and Sjolund, R.D. (1990). Sieve Elements. (Berlin: Springer-Verlag).
- Canny, M.J.P. (1975). Mass transfer. In Encyclopedia of Plant Physiology, Vol. 1, M.H. Zimmermann and J.A. Milburn, eds (Berlin: Springer-Verlag), pp. 139–153.
- Cronshaw, J., and Sabnis, D.D. (1990). Phloem proteins. In Sieve Elements, H.D. Behnke and R.D. Sjolund, eds (Berlin: Springer-Verlag), pp. 257–283.
- Esau, K. (1969). The Phloem. Encyclopedia of Plant Anatomy, Vol. 5 (Berlin: Borntraeger).
- Esau, K. (1978). Developmental features of the primary phloem in *Phaseolus vulgaris* L. Ann. Bot. **42**, 1–13.
- Esau, K., and Cronshaw, J. (1967). Tubular components in cells of healthy and tobacco mosaic virus-infected *Nicotiana*. Virology **33**, 26–35.
- Esau, K., and Gill, R.H. (1972). Nucleus and endoplasmic reticulum in differentiating root protophloem of *Nicotiana tabacum*. J. Ultrastruct. Res. **41**, 160–175.
- Evert, R.F. (1990). Dicotyledons. In Sieve Elements, H.D. Behnke and R.D. Sjolund, eds (Berlin: Springer-Verlag), pp. 103–137.
- Evert, R.F., and Derr, W.F. (1964). Callose substance in sieve elements. Am. J. Bot. **51**, 552–559.
- Evert, R.F., Tucker, C.M., Davis, J.D., and Deshpande, B.P. (1969). Light microscope investigation of sieve element ontogeny and structure in *Ulmus americana*. Am. J. Bot. **56**, 999–1017.
- Evert, R.F., Eschrich, W., and Eichhorn, S.E. (1973). P protein distribution in mature sieve elements of *Cucurbita maxima*. Planta **109**, 193–210.
- Fensholt, D.S. (1957). The bioelectric potentials of plants and their functional significance. I. An electrokinetic theory of transport. Can. J. Bot. **35**, 573–582.
- Fisher, D.B. (1975). Structure of functional soybean sieve elements. Plant Physiol. **56**, 555–569.
- Fisher, D.B., Wu, Y., and Ku, M.S.B. (1992). Turnover of soluble proteins in the wheat sieve tube. Plant Physiol. **100**, 1433–1441.
- Giaquinta, R.T., and Geiger, D.R. (1973). Mechanism of inhibition of translocation by localized chilling. Plant Physiol. **51**, 372–377.
- Goodall, H., and Johnson, M.H. (1982). Use of carboxyfluorescein diacetate to study formation of permeable channels between mouse blastomers. Nature **295**, 524–526.
- Grignon, N., Touraine, B., and Durand, M. (1989). 6(5)Carboxyfluorescein as a tracer of phloem sap translocation. Am. J. Bot. **76**, 871–877.
- Hartig, T. (1837). Vergleichende Untersuchungen über die Organisation des Stammes der einheimischen Waldbäume. Jahresber. Fortschr. Forstwiss. Forstl. Naturkd. **1**, 125–168.
- Hartig, T. (1854). Über die Querscheidewände zwischen den einzelnen Gliedern der Siebröhren in *Cucurbita pepo*. Bot. Z. **12**, 51–54.
- Hartig, T. (1860). Beiträge zur physiologischen Forstbotanik. Allgemeine Forst- u. Jagdzeitschrift **36**, 257–261.
- Hayes, P.M., Patrick, J.W., and Offler, C.E. (1987). The cellular pathway of radial transfer of photosynthates in stems of *Phaseolus vulgaris* L.: Effects of cellular plasmolysis and *p*-chloromercuribenzene sulphonic acid. Ann. Bot. **59**, 635–642.
- Johnson, R.P.C., Freundlich, A., and Barclay, G.F. (1976). Transcellular strands in sieve tubes; What are they? J. Exp. Bot. **101**, 1117–1136.
- Kempers, R., and van Bel, A.J.E. (1997). Symplasmic connections between sieve element and companion cell in the stem of *Vicia faba* L. have a molecular exclusion limit of at least 10 kD. Planta **201**, 195–201.
- Kempers, R., Ammerlaan, A., and van Bel, A.J.E. (1998). Symplasmic constriction and ultrastructural features of the sieve element/companion cell complex in the transport phloem of apoplasmatically and symplasmatically phloem loading species. Plant Physiol. **116**, 271–278.

- Kollmann, R.** (1973). Cytologie des phloems. In *Grundlagen der Cytologie*, G.C. Hirsch, H. Ruska, and P. Sitte, eds (Jena, Germany: Fischer), pp. 479–505.
- Lawton, D.M.** (1978a). P protein crystals do not disperse in uninjured sieve elements in roots of runner bean (*Phaseolus multiflorus*) fixed with glutaraldehyde. *Ann. Bot.* **42**, 353–361.
- Lawton, D.M.** (1978b). Ultrastructural comparison of the tailed and tailless P protein crystals respectively of runner bean (*Phaseolus vulgaris*) and garden pea (*Pisum sativum*) with tilting stage electron microscopy. *Protoplasma* **97**, 1–11.
- Münch, E.** (1930). *Die Stoffbewegung in der Pflanze*. (Jena, Germany: Fischer).
- Nakamura, S., Hayashi, H., Mori, S., and Chino, M.** (1993). Protein phosphorylation in the sieve tubes of rice plants. *Plant Cell Physiol.* **34**, 927–933.
- Oparka, K.J., and Johnson, R.P.C.** (1978). Endoplasmic reticulum and crystalline fibrils in the root protophloem of *Nymphoides peltata*. *Planta* **143**, 21–27.
- Oparka, K.J., Viola, R., Wright, K.M., and Prior, D.A.M.** (1992). Sugar transport and metabolism in potato tuber. In *Carbon Partitioning within and between Organisms*, C.J. Pollock, J.F. Farrar, and A.J. Gordon, eds (Oxford, UK: BIOS), pp. 91–114.
- Oparka, K.J., Duckett, C.M., Prior, D.A.M., and Fisher, D.B.** (1994). Real-time imaging of phloem unloading in the root tip of *Arabidopsis*. *Plant J.* **6**, 759–766.
- Palevitz, B.A., and Newcomb, E.H.** (1971). The ultrastructure and development of tubular and crystalline P protein in the sieve elements of certain papilionaceous legumes. *Protoplasma* **72**, 399–426.
- Patrick, J.W., and Offler, C.E.** (1996). Post-sieve element transport of photoassimilates in sink regions. *J. Exp. Bot.* **47**, 1165–1177.
- Rhodes, J.D., Thain, J.F., and Wildon, D.C.** (1996). The pathway for systemic electrical signal conduction in the wounded tomato plant. *Planta* **200**, 50–57.
- Roberts, C.J., Raymond, C.K., Yamashiro, C.T., and Stevens, T.H.** (1991). Methods to studying the yeast vacuole. *Methods Enzymol.* **194**, 644–661.
- Robidoux, J., Sandborn, E.B., Fensom, D.S., and Cameron, M.L.** (1973). Plasmatic filaments and particles in mature sieve elements of *Heracleum sphondylium* under the electron microscope. *J. Exp. Bot.* **79**, 349–359.
- Salisbury, F.B.** (1996). *Units, Symbols, and Terminology for Plant Physiology*. (Oxford, UK: Oxford University Press).
- Spanner, D.C.** (1958). The translocation of sugar in sieve tubes. *J. Exp. Bot.* **9**, 332–342.
- Spanner, D.C.** (1970). The electroosmotic theory of phloem transport in the light of recent measurements of *Heracleum* phloem. *J. Exp. Bot.* **21**, 325–334.
- Spanner, D.C.** (1978). Sieve-plate pores, open or occluded? A critical review. *Plant Cell Environ.* **1**, 7–20.
- Thaine, R.** (1961). Transcellular strands and particle movement in mature sieve tubes. *Nature* **192**, 772–773.
- Thaine, R.** (1962). A translocation hypothesis based on the structure of plant cytoplasm. *J. Exp. Bot.* **13**, 152–160.
- Thaine, R.** (1969). Movement of sugars through plants by cytoplasmic pumping. *Nature* **222**, 873–875.
- Thorsch, J., and Esau, K.** (1981a). Changes in the endoplasmic reticulum during differentiation of a sieve element in *Gossypium hirsutum*. *J. Ultrastruct. Res.* **74**, 183–194.
- Thorsch, J., and Esau, K.** (1981b). Nuclear degeneration and the association of endoplasmic reticulum with the nuclear envelope and microtubules in maturing sieve elements of *Gossypium hirsutum*. *J. Ultrastruct. Res.* **74**, 195–204.
- Toth, P.T., Bindokas, V.P., Bleakman, D., Colmers, W.F., and Miller, R.J.** (1993). Mechanism of presynaptic inhibition by neuropeptide Y at sympathetic nerve terminals. *Nature* **364**, 635–638.
- van Bel, A.J.E.** (1995). The low profile directors of carbon and nitrogen economy in plants: Parenchyma cells associated with translocation channels. In *Plant Stems: Physiology and Functional Morphology*, B.L. Gartner, ed (San Diego, CA: Academic Press), pp. 205–222.
- van Bel, A.J.E., and Kempers, R.** (1991). Symplastic isolation of the sieve element-companion cell complex in the phloem of *Ricinus communis* and *Salix alba* stems. *Planta* **183**, 69–76.
- van Bel, A.J.E., and van Rijen, H.V.M.** (1994). Microelectrode-recorded development of the symplastic autonomy of the sieve element/companion cell complex in the stem phloem of *Lupinus luteus* L. *Planta* **192**, 165–175.
- van der Schoot, C., and van Bel, A.J.E.** (1989). Glass microelectrode measurements of sieve tube membrane potentials in internode discs and petiole strips of tomato (*Solanum lycopersicum* L.). *Protoplasma* **149**, 144–154.
- van der Schoot, C., and van Bel, A.J.E.** (1990). Mapping membrane potentials and dye coupling in internodal tissues of tomato (*Solanum lycopersicum* L.). *Planta* **182**, 9–21.
- Walsh, M.A., and Popovich, T.M.** (1977). Some ultrastructural aspects of metaphloem sieve elements in the aerial stem of the holoparasitic angiosperm *Epifagus virginiana* (Orobanchaceae). *Am. J. Bot.* **64**, 326–336.
- Wang, H.L., Offler, C.E., Patrick, J.W., and Ugalde, T.D.** (1994). The cellular pathway of photosynthate transfer in the developing wheat grain. I. Delineation of a potential transfer pathway using fluorescent dyes. *Plant Cell Environ.* **17**, 257–266.
- Wang, N., and Fisher, D.B.** (1994). The use of fluorescent tracers to characterize the post-phloem transport pathway in maternal tissue of developing wheat grains. *Plant Physiol.* **104**, 17–27.
- Wergin, W.P., and Newcomb, E.H.** (1970). Formation and dispersal of crystalline P protein in sieve elements of soybean (*Glycine max* L.). *Protoplasma* **71**, 365–388.
- Wright, K.M., and Oparka, K.J.** (1996). The fluorescent probe HPTS as a phloem-mobile, symplastic tracer: An evaluation using confocal laser scanning microscopy. *J. Exp. Bot.* **47**, 439–445.
- Yin, Z.H., Neimanis, S., Wagner, U., and Heber, U.** (1990). Light-dependent pH changes in leaves of C3 plants. *Planta* **182**, 244–252.